AIAA JOURNAL
Vol. 46, No. 4, April 2008

Placement Optimization of Distributed-Sensing Fiber-Optic Sensors Using Genetic Algorithms

Jing Li,* Rakesh K. Kapania,† and William B. Spillman Jr.‡
Virginia Polytechnic Institute and State University, Blacksburg, Virginia 24061-0203

DOI: 10.2514/1.25090

In this paper, we present methodology for the placement optimization of both discretely and continuously distributed fiber-optic sensors in which many point or quasi-point sensors can be multiplexed along a single optical fiber. A unified sensor performance metric is defined for vibration monitoring and fault detection as the integration/summation of a weighted functional of some strain measure over the optical fiber length for both discretely and continuously distributed fiber-optic sensors. The optical fiber is represented by a nonuniform rational B-splines curve. The design variables include the control point coordinates of the nonuniform rational B-splines curve and the arclength coordinates of the point sensing element positions along the fiber. The constraints common to all kinds of optical sensors include the maximum fiber length and maximum allowed initial curvature. The constraints are treated as the exact penalty functions in the fitness function for any genetic algorithm. For discretely distributed fiber-optic sensors, we briefly show by an example how to use a genetic algorithm-based traveling salesman problem solver to optimally connect those optimally distributed sensors using one single optical fiber by minimizing the total fiber length. For continuously distributed fiber-optic sensors, two sets of examples are given as applications to fluttering or vibrating panels in aerospace engineering and a clinical smart bed for patient vital signal monitoring in biomedical engineering. In both cases, the integrating bend-sensing fiber-optic sensors are used.

Nomenclature

F	=	functional of a strain measure
$\mathbf{i}$	=	unit basis vector along a coordinate axis
L	=	arclength of a fiber or curve
l	=	length or width of a rectangular panel or mattress
$N_{i,q}$	=	B-spline basis functions
N_s	=	number of sensing elements or sensors
n	=	number of control points
P	=	perturbation
$\mathbf{P}$	=	position vector (array) of point(s)
p	=	penalty factor
$R_{\min}$	=	minimum curvature radius
s	=	arclength coordinate
t	=	time
w	=	weight
X	=	coordinate component in X axis
Y	=	coordinate component in Y axis
Z	=	coordinate component in Z axis
α	=	constant to scale the fitness
Δ	=	increment or gauge length
ϵ	=	generalized strain measure
ε	=	axial strain
θ	=	angular change
θ_d	=	angular distance
κ	=	curvature
ξ	=	nondimensional arclength coordinate or parameter
ω	=	angular frequency

Subscripts

A	=	amplitude
i	=	variable number for control points
j	=	variable number for sensing elements or sensors
q	=	variable number for polynomial degrees
0	=	initial state or starting point

Superscripts

L	=	lower bound
U	=	upper bound

I. Introduction

SENSOR placement or sensor location design is an important issue that engineers must address in solving problems like identification, analysis, control, and health monitoring of various structures. Such structures include aerospace vehicles, bridges, and offshore platforms, as well as human bodies in many applications in biomechanical engineering. There are often many issues related to sensor placement. For example, the number of available sensors is limited and their positions essentially fixed in service [1,2]. In such situations, sensor placement becomes a critical issue which governs the success and failure of the desired mission.

Although there are many types of sensors/actuators for structural health management technology for aerospace and nonaerospace vehicles, including fiber-optic sensors, active and passive acoustic sensors, electromagnetic sensors, wireless sensing systems, microelectromechanical systems (MEMS), and nanosensors [3], the algorithms for optimal placement of actuators and sensors appear to be very similar regardless of the application [4]. All these problems can be posed as selecting a subset of locations from a large set of candidate locations [4]. The approaches differ only in their choice of objective function and optimization algorithm. Therefore, it is useful to review some literature on sensor placement in other fields to deal with the sensor placement for a specific application.

Methods have been developed to optimally place sensors to address the control and identification of dynamic structures. Yu and Seinfeld [5] developed the observability and optimal location of

Presented as Paper 4334 at the 10th AIAA/ISSMO Multidisciplinary Analysis and Optimization Conference, Albany, New York, 30 August–1 September 2004; received 27 May 2006; revision received 28 September 2007; accepted for publication 1 October 2007.

*Graduate Research Assistant, Department of Aerospace and Ocean Engineering; currently Research Associate, Department of Mechanical Engineering, Oakland University, Rochester, MI 48309; li2@oakland.edu. Member AIAA.

†Professor, Department of Aerospace and Ocean Engineering; rkapania@vt.edu. Associate Fellow AIAA.

‡Associate Director, Fiber & Electro-Optic Research Center; wspillma@yahoo.com.

measurements for a class of linear distributed parameter systems by minimizing the trace of the steady-state covariance matrix (CM) of the state estimates. Shah and Udwadia [6] formulated and presented methodology for the problem of optimally positioning sensors in lumped and distributed parameter dynamic systems for the purpose of system identification from time-domain input–output data. They used a linear relation between small perturbations in a finite-dimensional representation of the system parameters and a finite sample of observations of the system time response to approximately determine the CM of the parameter estimates, and optimize the locations of a given number of sensors by minimizing a suitable norm of the CM. Udwadia and Garba [7] dealt with an optimal sensor placement method for structural identification. They decoupled the optimization and the identification using the concept of an efficient estimator for which the CM of the parameter estimates is inversely proportional to the Fisher information matrix (FIM). They demonstrated that maximizing the FIM would also minimize the CM which provides the best estimate of the structural stiffness parameter difference, and brought the method of linear effective independence (EI) between the modes. Kammer [8] proposed an EI algorithm based on the contribution of each sensor location to the linear independence of the identified modes. The initial candidate set of sensor locations was quickly reduced to the number of available sensors. Using the EI method for the error theory, Kammer [9] studied the effect of sensor error on sensor placement for independent identification of a set of selected target modes. Kammer and Brillhart [10] studied optimal sensor placement for modal identification using system-realization methods. The sensor placement method maximized the spatial independence and signal strength of targeted mode shapes by maximizing the determinant of an associated FIM. Kirkegaard and Brincker [11] studied the influences of both the measurements as statistically dependent random variables and the noise of the measurement on the optimal locations of sensors for parametric identifications of structural systems. The optimal sensor locations were determined by maximizing the determinant of the FIM. They demonstrated through a vibrating simply supported beam under a transverse random load that it is important to consider the statistical dependency between the measurements for the optimal sensor placement while the optimal sensor locations are less sensitive to the noise-to-signal ratio within an increasing number of sensors. Meo and Zumpano [12] considered the problem of locating sensors on a bridge structure with the aim of maximizing the data information so that structural dynamic behavior could be fully characterized. Mode shape displacements were taken as the measured data set. Six different optimal sensor placement techniques, three based on the maximization of the FIM, one on the properties of the CM coefficients, and two on energetic approaches, were investigated. Li et al. [13] found a connection between EI and modal kinetic energy (MKE) methods for sensor placement for the problem of dynamic testing, damage identification, and structural health monitoring. They concluded that EI is an iterated version of MKE with reorthonormalized mode shapes regardless of mass distribution of a structure. If previous EI algorithms are based on sensor set reduction from a large number of candidate sensors, Kammer [14] also presented an EI-based sensor placement method to expand a specified set of a few sensors to the desired numbers of sensors.

Sensor placement for fault or damage detection is critically important for structural health monitoring. Watanabe et al. [15] designed a reduced order time-varying linear observer for full state estimation and obtained the optimum sensor sites by an exhaustive search to minimize the observation cost for fault detection. Hemez and Farhat [16] based on the strain energy contribution of the structure using a variant form of the EI method to optimally place sensors for structure damage detection. Cobb and Liebst [17] and Shi et al. [18] prioritized the sensor locations according to their ability to localize structural damage based on the eigenvector sensitivity method from test modal data. Worden and Burrows [19] based their research on the curvature data and used a number of different methods, such as an heuristic method based on iterative insertion/deletion of sensors, genetic algorithms, and simulated annealing, to determine sensor distributions for fault diagnosis. Guo et al. [2] modeled small damage by the reduction of structural stiffness, therefore, the mode shape and eigenvalue change due to damage. The performance function was the summation of FIMs for all possible mode shapes with selected degree of freedoms associated with sensors. Patan and Patan [20] developed an approach to fault detection in distributed systems based on the maximization of the power of a parametric hypothesis test, and determined the optimal locations of sensors using the performance index operating on the FIM. Papadimitriou et al. [21] presented statistical methodology to optimally place sensors in a structure for damage detection and localization. The optimal sensor locations were determined by minimizing the information entropy of the uncertainty in the model parameters over the set of possible sensor configurations using a genetic algorithm (GA).

Because of its capability as both sensors and actuators, the piezoelectric material-based shape or placement optimization has been an active field for more than one decade. Padula and Kincaid [4] provided a survey of actuator and sensor placement problems from a wide range of engineering disciplines (both aerospace and nonaerospace engineerings) and a variety of applications. Combinatorial optimization methods were recommended as a means for identifying sets of actuators and sensors that maximize performance. Frecker [22] reviewed the work done in this area since 1999–2003, in addition to optimization strategies for topology design of actuators, actively controlled structures, and drive electronics design. Specifically, Gawronski and Lim [23] and Lim [24] employed a placement index based on the Hankel singular values (HSV) to determine the sensor and actuator locations that maximize observability and controllability criteria. The placement index was the summation of the approximate HSVs of individual observability and controllability pairs. Friswell [25] dealt with the design of both discrete and continuously distributed piezoelectric actuators and sensors for modal responses, with finite element-based beams as example. The width of the distributed sensor was approximated using the shape functions. The sensor output was the sum of the contributions of the elements. Mukherjee and Joshi [26] used a gradientless iterative technique to design the shape of piezoelectric actuators to achieve the desired shape of the structure by minimizing the quadratic measure of global displacement residual error between the desired and current structural configurations.

Though fiber-optic sensors have been identified as the leading candidate technology for meeting the requirement of minimal weight penalty [27], little work on placement optimization of fiber-optic sensors has been presented in the literature. Davis et al. [28] used a wavelength division multiplexed optic fiber Bragg grating (FBG) array to sense the structural vibration mode by monitoring strain at multiple points along a single fiber path. The placement of the sensors was determined by the locations of nodal points in the shapes of the first three vibration modes. Gill [29] reconstructed optical FBG sensor strain distributions and optimized discrete sensor locations for a plate damage detection using a GA. The fitness function was the summation of the entries of an assigned weight matrix. Tsamasphyros et al. [30–32] numerically investigated the optimum embedded or through-thickness locations of optical FBG sensor patches for the health monitoring of composite bonded laminate or metal plates.

Other methods or topics on sensor placement optimization could also be found in the literature. Miller [33] computed a Gaussian quadrature formula using the functional gain as a weight function, and thought that the nodes of the quadrature formula gave the optimal locations for sensors. Hiramoto et al. [34] used the explicit solution of the algebraic Riccati equation to determine the optimal sensor/actuator placement for active vibration control. Wouwer et al. [35] presented an optimality criterion for the selection of optimal sensor locations in distributed parameter systems; the criterion was maximizing the Gram determinant of the sensor responses or the parameter sensitivity functions to achieve their independence. Thite and Thompson [36] selected response measurement locations for force identification by minimizing condition numbers of the matrix of transfer functions to be inverted.

Because of their capability to handle discrete design variables and search for global solutions without using gradient information, GAs have been used in sensor placement-type problems [1,2,4,21,37], sometimes combined with gradient-based methods [1,4]. Yao et al. [37] demonstrated that GAs obtained more superior sensor placements than the iterative EI methods, which are FIM based. Therefore, the EI methods usually cannot find the global solution. Kirkegaard and Brincker [11] gave illustrative figures showing the multiple maxima for the determinant of the FIM via sensor locations. Abdullah et al. [1] addressed the necessity to use GAs for placement of sensors/actuators on civil structures, the members of which are usually discrete and therefore only discrete locations are available for sensors/actuators. Guo et al. [2] presented an improved GA for the global and constrained optimization of sensor locations for structural health monitoring systems. The performance function was based on damage detection. To overcome the inefficiency due to infeasible solutions to the problem, some improved strategies were used, such as crossover based on identification code, mutation based on two gene bits, and improved convergence.

In early GA researches, the genetic representation of a chromosome or a solution was limited to binary digits [38,39], but problem representation has been the subject of much investigation.[§] It has been shown that more natural representations are more efficient and produce better solutions [39]. One useful representation of an individual or chromosome for function optimization involves genes or variables from an alphabet of floating point numbers with values within the variables' upper and lower bounds. Michalewicz [39] has done extensive experimentation comparing real-valued and binary GAs and showed that the real-valued GA is an order of magnitude more efficient in terms of CPU time. He also showed that a real-valued representation moves the problem closer to the problem representation which offers higher precision with more consistent results across replications [39]. Along this line, Zhang et al. [40] presented a novel float-encoded GA and applied it to the optimal control of flexible smart structures bonded with piezoelectric actuators and sensors.

This paper presents a study of placement optimization of a class of spatially distributed-sensing fiber-optic sensors for fault detection and vibration monitoring using GAs. The sensor performance metric (SPM) can be expressed as the summation or integration of the contributions of all individual sensing elements along the fiber cable. This summation nature of the sensor performance is common for many fault detection and vibration monitoring applications of discrete sensors [2,23,24,29] and continuously distributed sensors [41–51]. Specifically, when strain sensing fiber optical sensors are considered, the individual contribution of each sensing element will be a function of some strain measure or the perturbation of the strain measure. The reported integrating axial strain fiber-optic sensors for vibration monitoring or control include two-mode modal domain fiber-optic sensors, which have a sinusoidal relation between the sensed intensity and integrated axial strain [43,44,46,47] for a large perturbation but a linear relation for a small perturbation. Multimode speckle-pattern-based integrating axial/bending strain fiber-optic sensors for vibration applications include statistical-mode (STM) and high-order mode excitation (HOME) sensors [51,52]. A linear relation exists between the sensed intensity variation and the spatial perturbation. Many other strain sensing fiber-optic sensors also have potential uses for integrating sensing. The available fiber-optic bending sensors include the bending loss based [53–58], asymmetrical-core based [59], diameter local decreasing based [60], and multicore FBG based [61,62]. For axial strain, the single-core FBG based discrete or quasi-continuously distributed fiber-optic sensors are among the best choice. Therefore, it is necessary to present methodology for placement optimization of spatially distributed integrating fiber-optic sensors. To the best of our knowledge, there has been no published work in the literature along this line.

[§]Houck, C., Joines, J., and Kay, G. M., A Genetic Algorithm for Function Optimization: A Matlab Implementation: http://www.ie.ncsu.edu/mirage/GAToolBox/gaot/papers/gaotv5.ps, 1995 [retrieved Oct. 2004].

This preliminary yet pioneering study does not address the efficiency of the algorithms used, nor address a specific application, but addresses a general formulation and methodology. Illustrative examples include the placement optimization of discretely distributed fiber-optic sensors but address that of continuously distributed fiber-optic sensors. The latter includes a thin square plate with an assumed cylindrical bending deformation mode/case, a thin square plate of the same size with a dominant bisinusoidal deflection mode/case, and a thick "smart" bed with a local indentation formed by a human breathing and heart beating to demonstrate the existence of multiple solutions, and the capability of GAs to directionally and positionally place a distributed-sensing optical fiber. The sensing fiber cable is represented by a nonuniform rational B-splines (NURBS) curve [63] that is uniquely determined by a finite number of control points, and attached on the plate or smart bed surface in the examples though it can also be embedded into them. Though the plate examples are for aerospace engineering uses and the smart bed example is for clinical uses, the formulation and methodology are general for a wide application.

II. Description of the Problem

A. Sensor Performance Metric

If many strain sensors are multiplexed along a single optical fiber [27], a distributed optic fiber sensor of long gauge is formed, which may receive many signals from the distributed sensing. From those received signals, various meaningful information can be retrieved according to proper signal processing techniques. Each of the desired set of information has a sensor performance metric associated with it. The goal of placement optimization of sensors is to enhance those SPMs to gain as much reliable and robust information as possible.

Although Fisher's information-based SPMs are among the most popular, as mentioned in the Introduction, for this preliminary methodology study of placement optimization of distributed fiber-optic sensors, we choose to use a very simple *integrating* SPM, defined as the following integration of weighted functional of some strain measure $\epsilon(s, t)$ along the fiber curve of length L and arclength coordinate s:

$$\text{SPM}\,(t) = \int_0^L w(s) F[\epsilon(s,t)]\,\mathrm{d}s \tag{1}$$

where t is time.

Two examples of the weight function are

$$w(s) \neq 0 \quad \text{for } 0 \leq s \leq L \tag{2}$$

which means that Eq. (1) is for a continuously distributed fiber-optic sensor, and

$$w(s)\begin{cases} \neq 0 & \text{if } 0 \leq s_j^L \leq s = s_j \leq s_j^U \leq L \\ & \text{for } j = 1, 2, \ldots, N_s \\ =0 & \text{else} \end{cases} \tag{3}$$

which reduces Eq. (1) into a summation of N_s discrete sensors of gauge length $\Delta_j = s_j^U - s_j^L$:

$$\text{SPM}\,(t) = \sum_{j=1}^{N_s} \int_{s_j^L}^{s_j^U} w(s) F[\epsilon(s,t)]\,\mathrm{d}s \approx \sum_{j=1}^{N_s} w(s_j) F[\epsilon(s_j,t)]\Delta_j \tag{4}$$

which means that Eq. (1) can also be for a discretely distributed fiber-optic sensor (see Fig. 1).

When the discrete sensors are dense enough along the optic fiber, a quasi-continuously distributed optic fiber sensor is formed. On the other hand, an actual continuously distributed-sensing optic sensor consists of an infinite number of infinitesimal sensing fiber segments or elements connected together.

The two simplest forms of function $F(\epsilon)$ are

$$F(\epsilon) = \epsilon \tag{5}$$

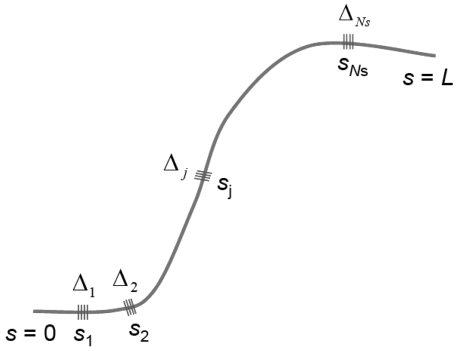

Fig. 1 A discretely distributed fiber-optic sensor.

and

$$F(\epsilon) = \|\epsilon\|_2 \tag{6}$$

where $\|\cdot\|_2$ denotes the L^2 norm. Then, Eq. (1) takes the following two forms:

$$\text{SPM}\,(t) = \int_0^L w(s)\epsilon(s,t)\,\mathrm{d}s \tag{7}$$

and

$$\text{SPM}\,(t) = \int_0^L w(s)\|\epsilon(s,t)\|_2\,\mathrm{d}s \tag{8}$$

The strain measure ϵ can be axial (ε), bending ($\Delta\kappa$), or some combination measure of the strain tensor components, or a *perturbation* of any of them. Clearly, for axial or bending strain, Eq. (7) is the net (weighted) fiber length or orientation change along the fiber length. The local elongation and shortening cancel along the fiber. The final value is independent to any intermediate strain state, but determined by the positions or orientations of the two ends.

The norm or absolute operator in Eq. (8), however, makes sure that any local elongation or shortening is a plus to the whole sensor performance. It is "path" dependent. In the bending case, it senses the angular *distance* if one traces the fiber from one end to the other. Any local perturbation can be sensed by the sensor.

The SPM in Eq. (1) and its reduced forms in Eqs. (4), (7), and (8) can be realized by most distributed fiber-optic strain sensors, as mentioned in the Introduction. Especially, the single-core and multicore FBG optic sensors are among the most suitable ones if the cost is not very important. For cost effective applications, the integrated axial strain of phase modulated two-mode modal domain fiber-optic sensors [43,44,46,47] takes the form of Eq. (7), and the spatial perturbation $P(t)$ of integrated axial and bending strain of STM and HOME sensors [51,52] takes the form of Eq. (8).

Because this study was initiated for a clinical smart bed application using the low cost STM and HOME sensors, some detail is given for a realization of the SPM in Eq. (8) using the two sensors though they can also be applied to advanced vehicle structures. The basic concept is that any disturbance to an optical fiber would produce a change in the optical signal that would indicate the disturbance. The spatially distributed-sensing fiber-optic sensors are based on the modulation of the modal distribution in multimode optical fibers. All the guided modes of the fiber are excited and then detected by a low cost digital camera (see Fig. 2). The output for the STM sensor is the sum of the absolute values of the change in light intensity on each of the pixels between each time frame, and proportional to the absolute value of the first time derivative of the integrated spatial perturbation along the fiber [51,52]. For the HOME sensor, the output is proportional to the integration of the absolute values of the bending strain [51,52]. In either case, the whole output of this distributed-sensing optical fiber is the sum of the output contributions of an infinite number of infinitesimal fiber segments. The contribution of each infinitesimal fiber segment to the output is proportional to its spatial perturbation $\mathrm{d}P$ that is the angular change of the fiber segment if the bending is dominant:

$$\mathrm{d}\,\theta_d = |\mathrm{d}\theta| = \|\Delta\kappa(s,t)\|_2\,\mathrm{d}s \tag{9}$$

Then, the total spatial perturbation of the whole distributed-sensing fiber-optic sensor is the integration of the absolute curvature change due to a given external perturbation over the whole fiber length L:

$$P(t) = \theta_d = \int_0^L \mathrm{d}\theta_d = \int_0^L \|\Delta\kappa(s,t)\|_2\,\mathrm{d}s \tag{10}$$

Therefore, the spatial perturbation $P(t) = \theta_d$, as a special form of SPM, represents the angular distance if one traces the fiber curve from one end to the other.

The curvature change or bending strain $\Delta\kappa(s,t)$ of the fiber segment $\mathrm{d}s$ can be retrieved from the deformation data of the structure that the optic fiber is attached to. In this preliminary study, we assume that the sensing optical fiber is attached onto the structural surface or embedded into the structure so that no slip motion occurs between the optical fiber and the structure. We further assume that the tangent, normal and binormal of the Frenet frame [63] are computable for both the fiber curves before and after the spatial perturbation. Then, the bending curvature can be retrieved according to the formula provided in the papers by Kapania and Li [64,65] and references therein.

B. Design Variables/Placement Representation

A distributed-sensing fiber-optic sensor consists of either an infinite number of infinitesimal sensing fiber segments or a finite number of sensing elements as quasi-point sensors. We here have two classes of placement design variables: the design variables that determine the fiber curve placement or shape, and the design variables that are the number of the sensing elements and their site locations along the fiber.

If we represent the *unperturbed* fiber curve using NURBS, which can be expressed mathematically by

$$\mathbf{P}\,(\xi) = \frac{\sum_{i=0}^{n} N_{i,q}(\xi) w_i \mathbf{P}_i}{\sum_{i=0}^{n} N_{i,p}(\xi) w_i} \quad \text{for } 0 \le \xi \le 1 \tag{11}$$

where q is the polynomial degree, $N_{i,q}$ are the B-spline basis functions, $\mathbf{P}_i(\xi) = X_i(\xi)\mathbf{i}_X + Y_i(\xi)\mathbf{i}_Y + Z_i(\xi)\mathbf{i}_Z$ are the *control points*, and the weights w_i of $\mathbf{P}_i$ are the last coordinates of homogeneous points $\mathbf{P}_i^w$ [63]. The control point coordinates $X_i(\xi)$, $Y_i(\xi)$, and $Z_i(\xi)$ are the design variables for a fiber curve placement, subject to side constraints:

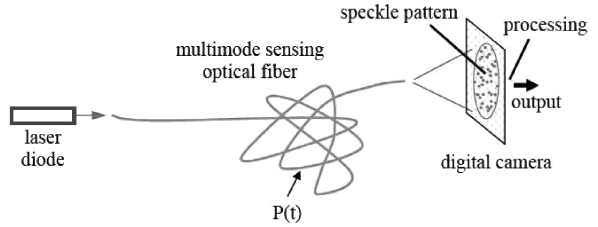

a) STM sensor $Output(t) \propto \dfrac{\mathrm{d}P(t)}{\mathrm{d}t}$

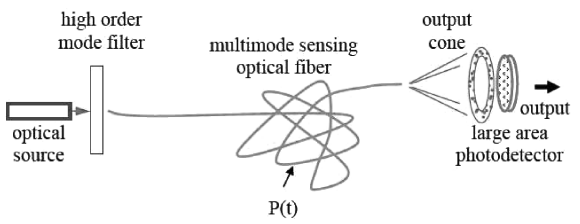

b) HOME sensor $Output(t) \propto P(t)$

Fig. 2 Multimode fiber-optic sensor schematic diagram.

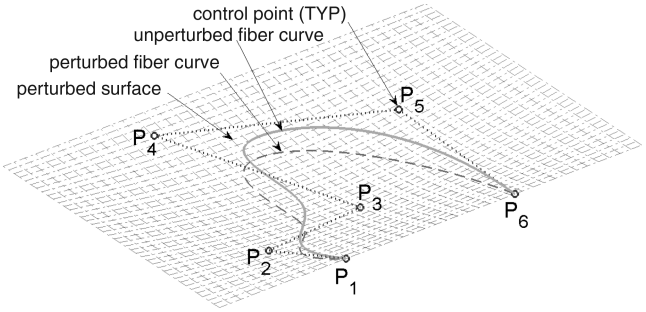

Fig. 3 An optical fiber placement represented by a NURBS curve. TYP = typical.

$$X_i^L \le X_i(\xi) \le X_i^U \qquad Y_i^L \le Y_i(\xi) \le Y_i^U \qquad Z_i^L \le Z_i(\xi) \le Z_i^U \tag{12}$$

Refer to Fig. 3 for a surface attached optical fiber placement represented by a NURBS curve with only six control points.

Refer to Eqs. (3) and (4). If N_s point or quasi-point sensors are multiplexed in a single optical fiber at positions s_j, the nondimensional site positions ξ_j, which determine the arclength site positions $0 \le s_j = s(\xi_j) \le L$ along the fiber curve, can be the design variables for sensor site positioning, subjected to the side constraints:

$$0 \le \xi_j \le 1 \tag{13}$$

When the point sensing elements along the optical fiber are dense enough so that the off-site physical parameters can be determined by the physical parameters measured by the on-site sensors through curve fitting or interpolation, those point sensors multiplexed along the optical fiber form a quasi-continuously distributed-sensing fiber-optic sensor. Then, the point sensors can be uniformly distributed along the fiber and their positions are no longer independent design variables. That is, there is no need to define extra positioning design variables for an infinite number of infinitesimal small sensing elements for a continuously distributed fiber-optic sensor, which is uniquely determined by the control points of a NURBS curve.

C. Constraints

For exactly sensing structural parameters, an optical fiber sensor should be either attached onto the structural surface or embedded into the structure. It is assumed that there is no slip nor debonding between the fiber and the sensed structure. Therefore, the deformation of the optical fiber can be retrieved from the deformation data of the sensed structure by interpolating.

For the panel and smart bed examples in this study, the optical fiber is attached onto the rectangular surface of a panel or mattress, and bilinear interpolation is used to retrieve the perturbed optical fiber position from the displacement data at the grid points, as shown in Fig. 3.

The control points of the NURBS curve for a fiber bounded according to Eq. (12) may be allowed to be placed outside of the panel or mattress surface, but the curve points of the optical fiber should always be bounded within the structure.

For a continuously distributed fiber-optic sensor, due to scaling nature [49], we might consider using a longer fiber-optic cable to get a better sensor performance. However, we may need to put a constraint on the fiber length due to cladding mode lost or laser power limit;for example, we can set $L \le L^U$, where the maximum length L^U is usually of the order of several meters if the fiber-optic sensor is bending based but could be much longer without adversely affecting the SPM for FBG based. In the latter case, the length of the optical fiber should be minimized to meet the minimum weight requirement.

A *microbend* design may be useful to enhance the sensor performance. The initial curvature or radius of the unperturbed optical fiber is, however, subject to the limitation due to *bending losses* [53–58,66]. Therefore, there is an upper bound constraint for the initial curvature $\kappa_0 \le \kappa_0^U$, where $\kappa_0^U = 1 \text{ rad}/R_{\min}$ may be of the order of $1 \text{ rad}/(15r)$ with r as the fiber radius. If the structural dimensions are much larger than the minimum curvature radius $R_{\min}$, the maximum curvature constraint can be temporarily ignored. Then, a sharp corner is allowed during placement optimization, but taken into account as the final finish after optimization, as shown in Fig. 4.

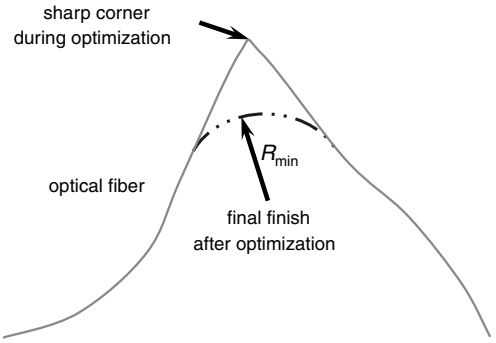

Fig. 4 Maximum initial curvature constraint treatment.

D. Fitness Function

In this paper, the fitness function for the GA is defined *effectively* in the sense of the exact penalty function method [67] to handle constraints:

$$\text{fitness} = \alpha \text{SPM} \cdot \left[1 - p_\kappa \max\left(\frac{\kappa_{0\max}}{\kappa_{0\max}^U} - 1, 0 \right) - p_L \max\left(\frac{L}{L^U} - 1, 0 \right) \right] \tag{14}$$

where the sensor performance metric SPM does not limit but could be any instance of Eq. (1). L and L^U are the current and maximum allowed lengths of the fiber curve, respectively. $\kappa_{0\max}$ and $\kappa_{0\max}^U$ are the maximum and the maximum allowed initial curvatures of the fiber curve, respectively. p_L and p_κ are the corresponding penalty factors, finite but large enough to draw a design point from the infeasible domain to the feasible domain. α is a scaling constant of the fitness to avoid numerical instability.

III. Examples

A. Homogeneous Rectangular Panel with Uniformly Distributed Damage Probability Density

There is a homogeneous rectangular panel of 200×100 cm^2 with a uniformly distributed damage probability density over the panel. It is desirable to optimally place a discrete FBG sensor array of 40 gratings of the same gauge size so that any actual damage on the panel can be identified and localized through monitoring the perturbation of the strain field, but the total length of the optical fiber that multiplexes the 40 FBG sensors is minimized.

Because there is no further a priori knowledge available than that of uniformly distributed damage probability density, we may use some optimal Latin hypercube sampling (LHS) as the optimality criterion to first place those 40 discrete FBG sensors because there is no upper bound set on the total length of the optical fiber. That is, the 40 FBG sensors will be placed at the optimal LHS points. A strain field metamodel could be built up using the measured strain data at those sensor sites. After the sensor sites are determined, we can use a traveling salesman problem (TSP) solver to optimally connect those sensor sites using a single fiber curve of minimal length. An optimal placement of a FBG sensor array and the corresponding design history are shown in Figs. 5 and 6, respectively.

The results were obtained in MATLAB. The random seed was set as rand('seed,'156789). As the discrete sensor sites, the 40 numbered optimal LHS points were obtained by invoking lhsdesign (40,2,'iterations,'25000).

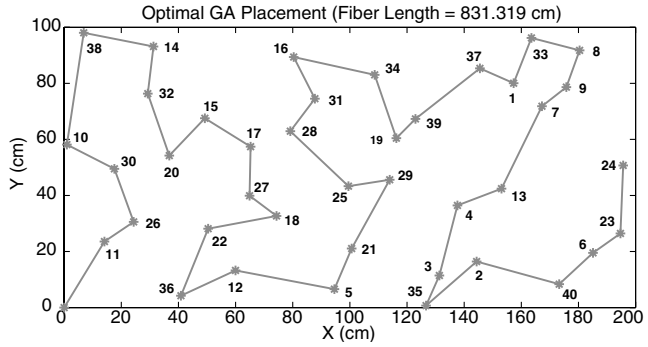

Fig. 5 An optimal placement of a FBG optic sensor array using optimal LHS design and a GA-based TSP solver.

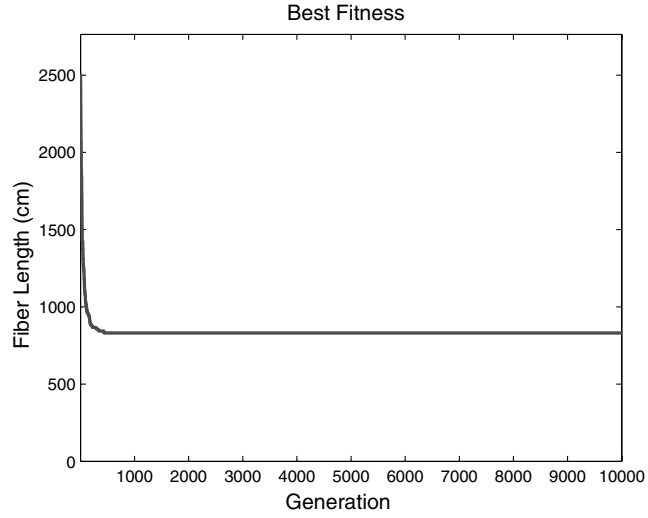

Fig. 6 GA design history of placement optimization of a FBG optic fiber using a GA-based TSP solver.

The GA-based TSP solver, "Traveling Salesman Problem—Genetic Algorithm" in the category of optimization[¶] developed by Joseph Kirk, was used. We modified it so that the salesman travels to every city exactly once, but does not need to return. Therefore, it allows one to place the optical fiber with one end of the fiber as a fixed lead (e.g., the left-bottom corner in this example), and the other end is free to be placed onto any sensor site. The default population size 100 and high mutation rate 0.8 were used. The crossover rate is built in the code and not an input parameter. The fiber curve length of the best solution in the initial population is more than 2500 cm but the minimal fiber length at termination is reduced to 831 cm. The initial curvature constraint can be enforced as a final finish according to Fig. 4.

The purpose of this example addresses the placement optimization of a single optical fiber that serves as the light pipe and multiplexes any set of discrete FBG sensors optimally placed by any mature optimization method for discrete sensors. It is shown that the GA-based TSP optimizer can serve this purpose to minimize the single fiber length. We point out here that if the couplers/dividers are used, the minimal-spanning tree solver can be used for the same purpose to obtain a shorter fiber length of more complex fiber-optic sensor arrays.

B. Continuously Distributed Integrating Fiber-Optic Sensor on a Square Panel for Vibration Monitoring

There is a square panel of 50×50 cm^2 with a single dominant harmonic vibration mode/case corresponding to the angular frequency ω. The in-plane strain is ignorable, and therefore, the panel is subject to a bending deformation. The integrating bending strain perturbation can then, according to Eq. (10), be expressed as

$$P(t) = \int_0^L \|\Delta\kappa_A(s)\sin\omega t\|_2\,\mathrm{d}s = P_A|\sin\omega t| \tag{15}$$

and its first time derivative is

$$\left|\frac{\mathrm{d}P(t)}{\mathrm{d}t}\right| = \omega P_A|\cos\omega t| \tag{16}$$

where the perturbation amplitude

$$P_A = \int_0^L \|\Delta\kappa_A(s)\|_2\,\mathrm{d}s \tag{17}$$

is the integrated bending curvature of the dominant deformation mode/case. Therefore, to enhance the sensor performance according to either Eq. (15) or Eq. (16), it is desirable to maximize P_A according to Eq. (17). Referring to Fig. 2, Eqs. (15) and (16) can be realized using not only STM/HOME sensors, but also quasi-continuously distributed bending sensors, including the multicore FBG-based sensors.

We consider two simple numerical cases using "The Genetic Algorithm Optimization Toolbox (GAOT)." GAOT, developed by Houck et al. [68], implements simulated evolution in the MATLAB environment using both binary and real representations, and is freely available online. The standard procedure we used for each generation is as follows:

1) Record the best, average, and standard deviation of the current population.

2) Select the individuals for reproduction according to normalized geometric distribution [68]. The probability to select the best is 0.08.

3) Reproduce children at random through arithmetic, heuristic, and simple crossovers [68] for given numbers of times to replace parents.

4) Mutate the population at random through uniform, boundary, nonuniform, multi-non-uniform mutations [68] for given numbers of times.

5) Replace the worst with the recorded best.

1. *Cylindrical Deformation Mode/Case*

The square plate is simply supported along the two opposite edges parallel to the X axis and free along the other two opposite edges parallel to the Y axis. The dominant deformation is assumed to be pure bending of a cylindrical shape. The bending strain/curvature is constant over the panel, and the maximum curvature $\Delta\kappa_{A\max}(s) = 0.0107$ rad/cm is along the Y axis and the maximum deflection is 3.4 cm. Therefore, an optimal placement of the optical fiber is any one with the optical fiber being aligned along the Y axis as possible as it can. The upper bound on the integrating bending curvature P_A is $\Delta\kappa_{A\max}L^U = 3.21$ rad/cm if $L^U = 300$ cm, which can be achieved when the maximum allowed initial curvature is ∞ and all control points are aligned onto a line parallel to the Y axis. There will be multiple solutions if the fiber length is allowed to be larger than the panel edge length of 50 cm.

The results of a placement optimization using GAOT are shown in Fig. 7 under the following setting. The optical fiber is represented by a NURBS curve with 20 control points, which are bounded within a square of 62.5×62.5 cm^2. The two ends of the distributed fiber-optic sensor are fixed at the midpoint of the edge on the X axis. Therefore, the 36 coordinates of 18 control points are design variables. The NURBS Toolbox developed by Spink [69] is used for NURBS calculations.

The bending curvature involves up to third order of finite differences of curve points using a "gradient" function in MATLAB. It may contain large numerical errors around the sharp corners of the curve. Therefore, the initial curvature constraint is enforced and removes any points at which the calculated bending curvatures exceed a given maximum curvature bound. The numerical errors on

[¶]Data available online at http://www.mathworks.com/matlabcentral/fileexchange/loadCategory.do [retrieved Aug. 2007].

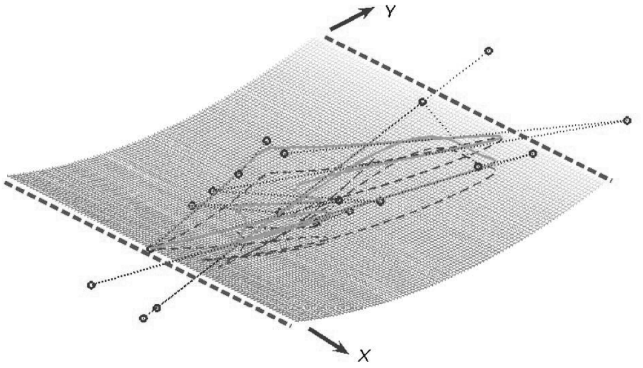

a) The optimal placement

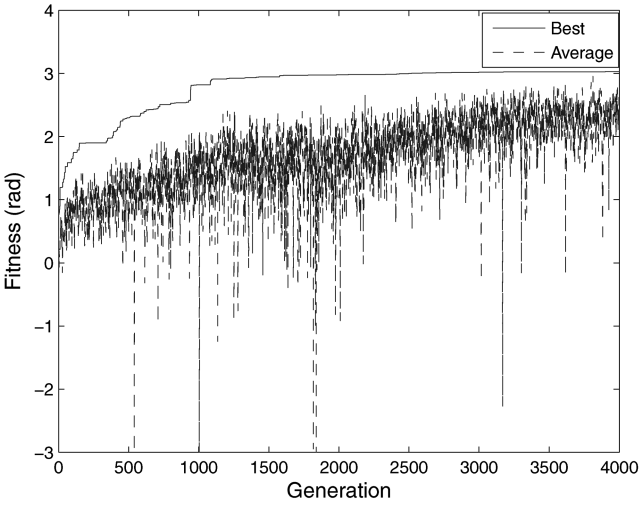

b) GA design history

Fig. 7 An optimal placement of a continuously distributed optic sensor on a square panel with a cylindrical deformation mode/case using GAOT.

the bending strain calculation may slow down the convergence and limit the capability to find the more exact optimal placement.

The parameters for GAOT are as follows.

For fitness in Eq. (14), $\alpha = 1$,

$$\text{SPM} = \theta_d = \int_0^L \|\Delta\kappa_{\text{A}}(s)\|_2 \, \text{d}s$$

$\kappa_{0\max}^U = 2$ rad/cm, $L^U = 300$ cm, and $p_\kappa = p_L = 1.5$.

The seed for random numbers is set as rand('seed,'156789). The population size is 20. The maximum number of generations for termination is 4000. The numbers of times for arithmetic, heuristic, and simple crossovers for a generation are all 1. The numbers of times for uniform, boundary, nonuniform, multi-non-uniform mutations for a generation are 2, 3, 2, and 2, respectively.

At the optimum after 4000 generations (a total of 30,578 function evaluations), the SPM is $\theta_d = 3.03$ rad, the maximum initial curvature is $\kappa_{0\max} = 1.95$ rad/cm, and the total fiber length is $L = 296.68$ cm. The two constraints are satisfied and the integrating bending curvature 3.03 rad is close to the upper bound value of 3.21 rad.

Figure 7 shows that the optical fiber after 4000 generations has been aligned closely in the orientation of the maximum bending curvature.

2. Bisinusoidal Deformation Mode/Case

The square panel is simply supported along all four edges. The dominant deformation is of a bisinusoisal shape $w = w_{\max} \sin(\pi/a)X \sin(\pi/a)Y$ with maximum deflection $w_{\max} = 3.4$ cm. The panel edge length is $a = 50$ cm. The panel bending curvature is not a constant (referring to Fig. 8 for the principal curvatures calculated using data at 400×400 grid points), but has a maximum curvature $(\pi/a)^2 w_{\max} = 0.0134$ rad/cm along the two diagonal lines. Therefore, we can fix the two ends of the optical fiber at the corners. It is apparent that there are multiple solutions because there are eight lines of symmetry for bending.

All other conditions are the same as the case of the cylindrical deformation mode/case, except that the population size is 40.

Figures 9 and 10 show the optimal placements after 2000 generations and design histories for the two ends fixed at two corners on the X axis, and at one corner, respectively.

For the case of the two ends fixed at two corners on the X axis, after 2000 generations (a total of 15,473 function evaluations), the SPM is $\theta_d = 2.88$ rad, the maximum initial curvature is $\kappa_{0\max} = 0.89$ rad/cm, and the total fiber length is $L = 298.65$ cm. The two constraints are satisfied.

Similarly, for the case of the two ends fixed at one corner, after 2000 generations (a total of 16,890 function evaluations), $\theta_d = 3.55$ rad, $\kappa_{0\max} = 0.35$ rad/cm, and $L = 298.59$ cm. The two constraints are satisfied.

It can be seen that the optimal placement in Fig. 9 is more dominated by the maximum principal curvature than the optimal placement in Fig. 10 but with a lower SPM.

C. STM/HOME Fiber-Optic Sensors for a Clinical Smart Bed for Patient Vital Signal Monitoring

The integrated smart bed [51,52] is a special smart structure developed for clinical use. The patient's vital signals are the

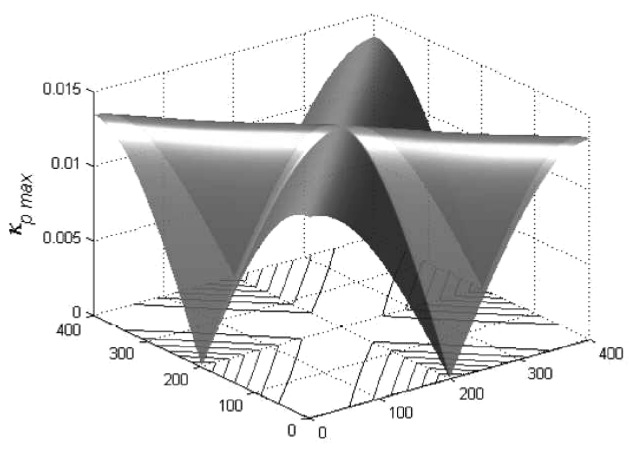

a) Maximum principal curvature κ_{pmax}

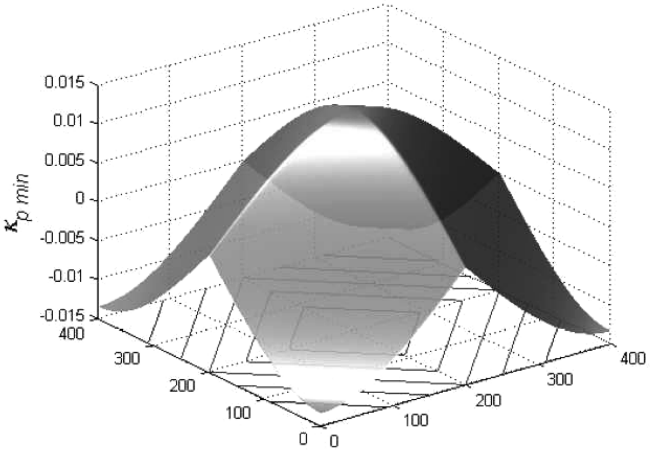

b) Minimum principal curvature κ_{pmin}

Fig. 8 Principal curvatures of the bisinusoidal deformation.

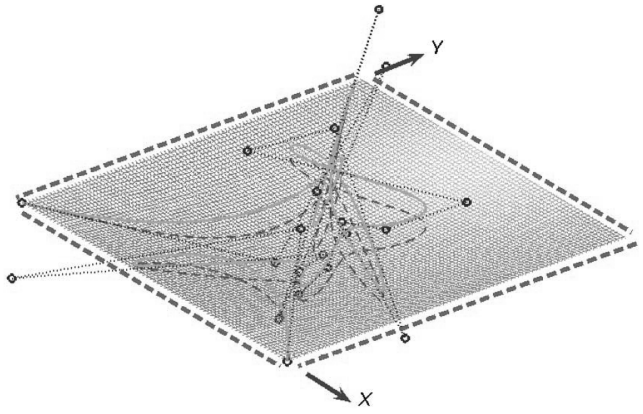

a) The optimal placement

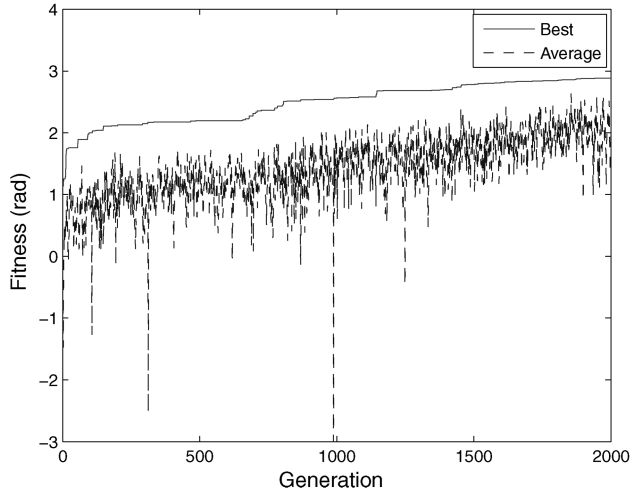

b) GA design history

Fig. 9 An optimal placement of a continuously distributed optic sensor on a square panel with a bisinusoidal deformation mode/case using GAOT.

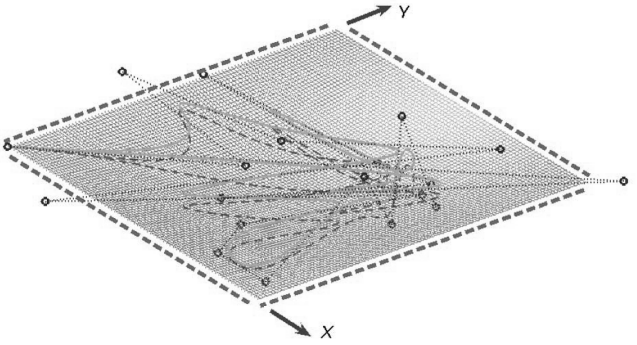

a) The optimal placement

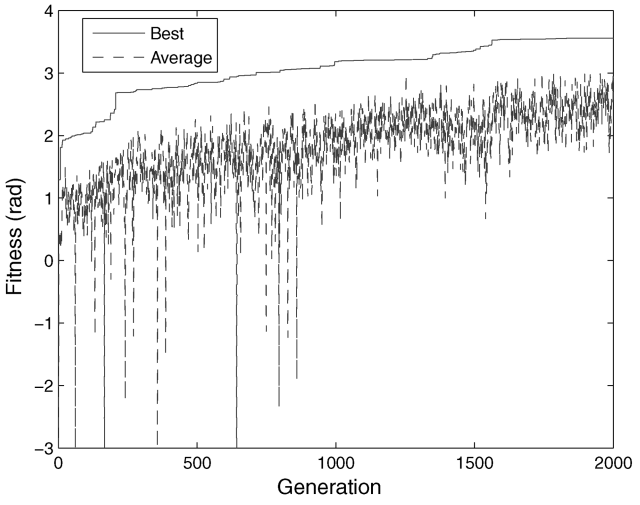

b) GA design history

Fig. 10 An optimal placement of a continuously distributed optic sensor on a square panel with a bisinusoidal deformation mode/case using GAOT.

vibrations monitored, including breath/heart beat rates, and the body movement and absence of the patient.

The low cost STM/HOME (referring to Fig. 11) sensors are considered for the smart bed. An interactive design tool "Java Tool for the Placement of Fiber-Optic Sensors" is developed for the placement optimization of the distributed-sensing fiber sensors. GAJIT, a simple Java genetic algorithms package by Faupel** is used to optimize the placement of the fiber NURBS curve.

1. Simple Breeding Algorithm

The simple breeding algorithm in GAJIT we used for the NURBS curve design is as follows:

1) Remove a percentage of the least fit designs through culling.

2) Preserve a percentage of the most fit designs unchanged (elitism).

3) Then breed the elite and the remainder at random according to the uniform distribution regardless of their fitnesses through two-point crossover and bitwise uniform mutation to fill out the rest of the next generation.

The relevant parameters for the GA are briefly defined as follows:

1) Culling rate: percentage deemed unfit for reproduction.

2) Elite rate: percentage of population carried forward unchanged from each generation.

3) Weight: the weighting a genetic operator has for the chances of it being selected.

**Data available online at http://www.micropraxis.com/gajit/index.html [retrieved Dec. 2003].

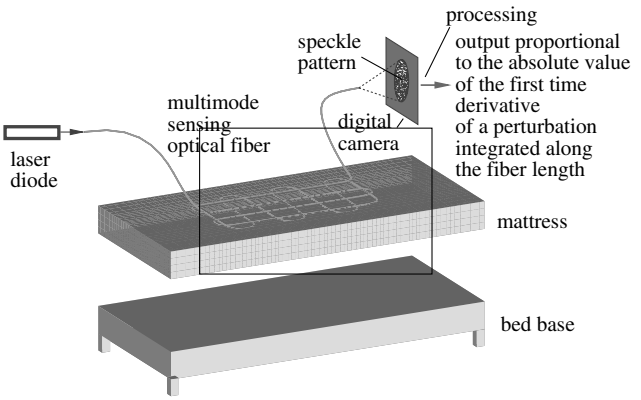

Fig. 11 A schematic diagram of the STM sensor for an integrated smart bed.

2. Coding/Decoding

GAJIT is binary coded but we can approximate the continuous design variables using discrete ones as illustrated through Fig. 12.

For the placement of the fiber-optic sensor, we can list the design variables into the array:

$$\mathbf{P} = \begin{bmatrix} 15.9677 & -7.379 \\ -9.5806 & 25.0887 \\ 28.7419 & 10.3306 \\ -15.9677 & -1.4758 \end{bmatrix} \tag{18}$$

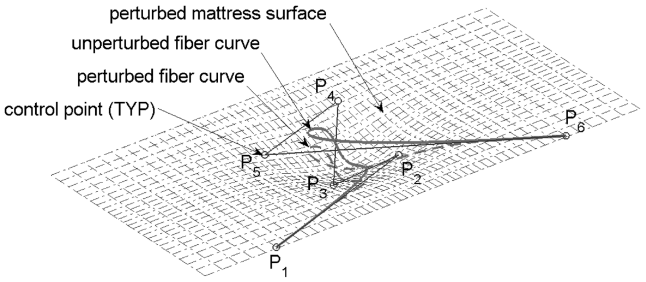

Fig. 12 A placement of a fiber-optic sensor on a smart bed mattress surface represented by a NURBS curve with six control points. The center of the mattress surface is the origin of the coordinate system.

in which each row is the coordinate pair (X, Y) of one of (four) designable control points of the fiber NURBS curve (the two ends are fixed). Scaling the coordinate pairs of $\mathbf{P}$ according to $-1 \le \bar{X} = 2X/l_X \le 1$ and $-1 \le \bar{Y} = 2Y/l_Y \le 1$ ($l_X = 198$ cm and $l_Y = 91.5$ cm are the length and width of the mattress, respectively), we have

$$\bar{\mathbf{P}} = \begin{bmatrix} 0.16129032258064502 & -0.16129032258064524 \\ -0.09677419354838712 & 0.5483870967741935 \\ 0.29032258064516125 & 0.22580645161290325 \\ -0.16129032258064524 & -0.032258064516129004 \end{bmatrix} \tag{19}$$

To code the eight coordinates using eight genes (gene size = 5) of a chromosome represented by a binary string, we can functionally use the relation

$$\bar{X}_{\text{integer}} = \text{floor}[(\bar{X} + 1) \times 2^{\text{gene size}-1}] \tag{20}$$

to obtain the following approximate integer representation:

$$\bar{\mathbf{P}}_{\text{integer}} = \begin{bmatrix} 18 & 13 \\ 14 & 24 \\ 20 & 19 \\ 13 & 15 \end{bmatrix} \tag{21}$$

Then, the corresponding binary representation is

Table 1 Mattress core hardness and calculated maximum deformations

Hardness range	E = Young′s modulus, N/cm^2	Maximum deflection, cm	Maximum nominal strain
Soft	1.213	15.0	0.909
Medium	1.493	12.2	0.739
Firm	1.765	10.3	0.624
Extra firm	2.041	8.92	0.541
Super firm	2.317	7.86	0.476

$$\bar{\mathbf{P}}_{\text{binary}} = \begin{bmatrix} 10010 & 01101 \\ 01110 & 11000 \\ 10100 & 10011 \\ 01101 & 01111 \end{bmatrix}_{\text{binary}} \tag{22}$$

which is internally represented by the chromosome string of length 40

$$[01111011011001110100110000111001101100 10]_{\text{binary}}$$

which represents a member of the population.

Reversing the above procedure, any chromosome $\bar{\mathbf{P}}_{\text{binary}}$ can be decoded back to its decimal counterpart $\bar{\mathbf{P}}$ for evaluation of the fitness of a chromosome.

3. *Numerical Results*

We choose a mattress of a standard size $198 \times 91.5 \times 16.5$ cm^3 ($78 \times 36 \times 6.5$ in.^{3}) for the illustrative example. The assumed *locally* perturbed surface is obtained by a 10% scaling of the calculated deformation of the soft cored mattress (Table 1[††]) using MSC.NASTRAN linear analysis under an assumed body pressure with the maximum value of 1.00 N/cm^2 as shown in Fig. 13. Obviously from Table 1, a linear analysis is not proper for the total mattress deformation although there will be no problem for the small perturbation we used for the sensor placement.

Only 25 control points of the fiber NURBS curve are used, the two ends of which are fixed.

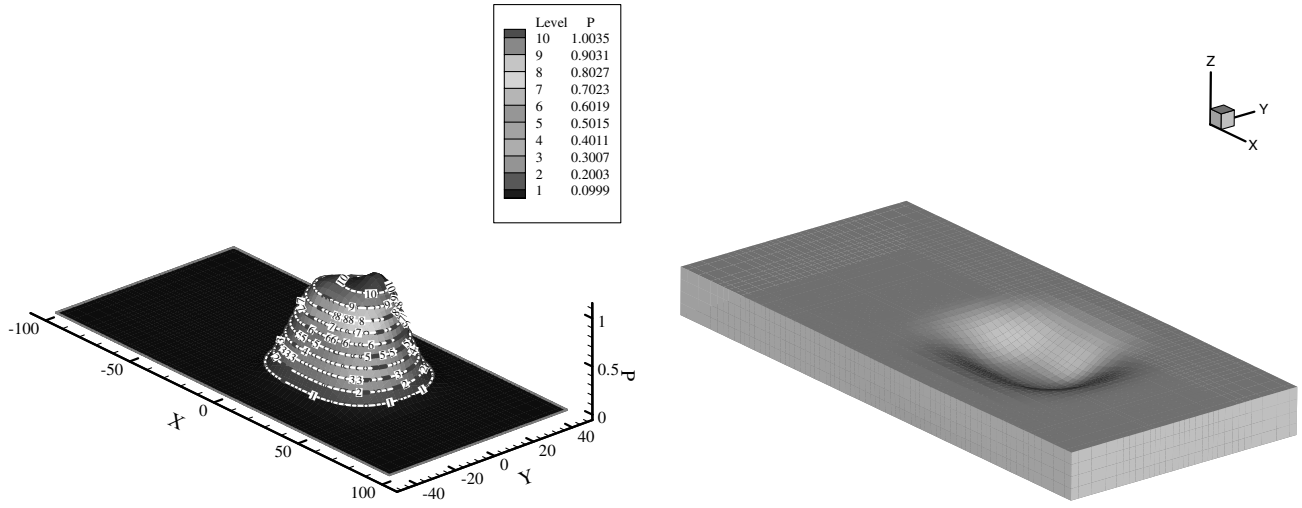

a) Body pressure **b) Deformation**

Fig. 13 Body pressure and deformation of the soft cored mattress. The pressure P has units of N/cm^2. FEM model: $70 \times 30 \times 4 = 8400$ brick elements for the mattress core; the cover is ignored.

[††]The typical values of Young's modulus E are calculated from http://www.flobeds.com/mattspec.htm. Poisson's ratio $\nu = 0.3$ for latex rubber foam is from Fig. 12 of [70].

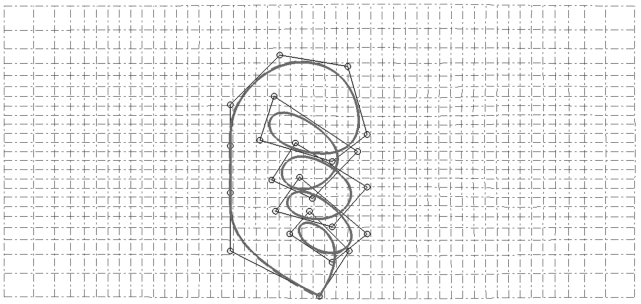

a) An initial placement: θ_d = 1.01rad; L = 358.95cm; κ_{0max} = 0.49 (rad/cm)

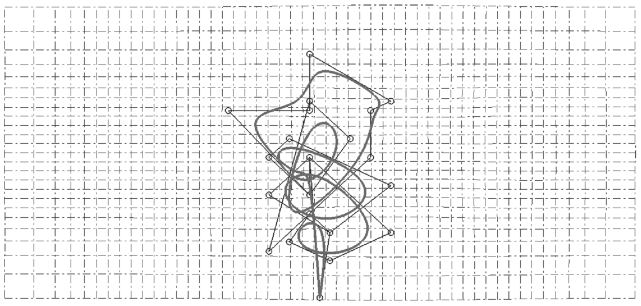

b) An 5000 generations: θ_d = 1.32rad; L = 386.33cm; κ_{0max} = 0.49 rad/cm

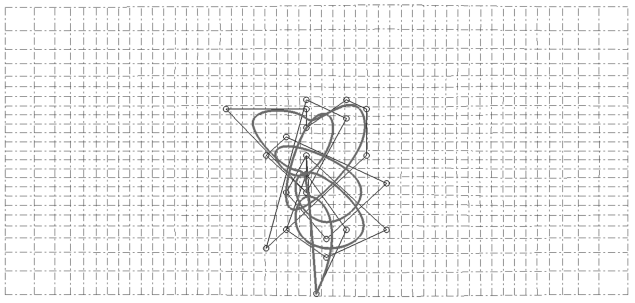

c) After 7000 generations: θ_d = 1.47rad; L = 386.09cm; κ_{0max} = 0.49 rad/cm

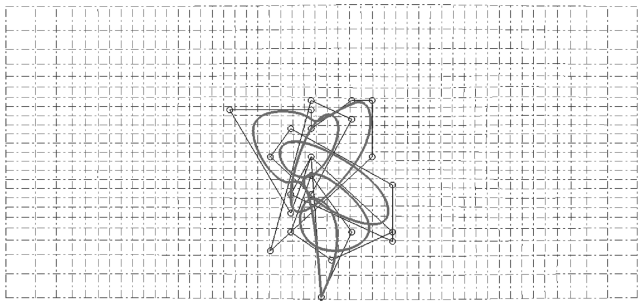

d) After 9000 generations: θ_d = 1.51rad; L = 399.99cm; κ_{0max} = 0.49 rad/cm

Fig. 14 Placement optimization history of a fiber-optic sensor for a smart bed by GA.

For the fitness in Eq. (14),

$$\text{SPM} = P_A = \int_0^L \|\Delta\kappa_A(s)\|_2 \, \mathrm{d}s$$

according to the perturbation amplitude in Eq. (17). $\alpha = 1/L^U$, $L^U = 400$ cm, $\kappa^U_{0\max} = 0.5$ rad/cm, $p_L = 4$, and $p_\kappa = 2$. For a GA search, elite rate, culling rate, and weight are 0.05, 0.2, and 0.1, respectively. The mutation rate for each bit of 40 bits is $1/40$.

Figure 14 shows the design history of the placement optimization of a statistical mode sensing (STH)/HOME-based fiber-optic sensor for the smart bed by GA. One of the 25 members in the initial population is artificially seeded and the control points of the rest are generated at random according to uniform distribution within the mattress surface area.

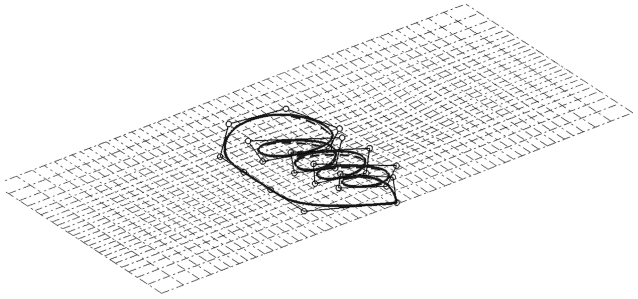

a) An initial placement. θ_d = 1.01 rad

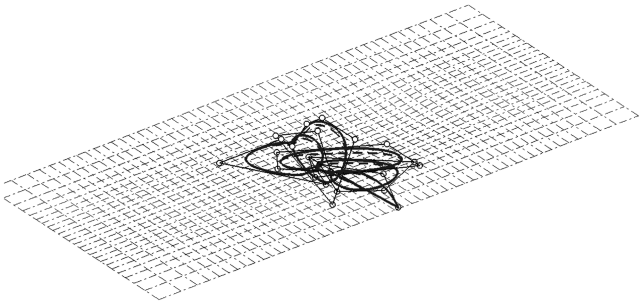

b) An updated placement after 9000 generations of GA iteration. θ_d = 1.51 rad

Fig. 15 A 3-D view of the initial placement and updated placement. The perturbed (dashed) and unperturbed (solid) fiber curve shapes of the optimal placement of the fiber-optic sensor.

It is shown that the preset initial placement of the fiber curve is feasible but with a lower sensor performance of 1.01 rad, a length of 358.95 cm, and maximum initial curvature of 0.49 rad/cm. After 9000 generations of the GA iteration, an updated placement is achieved, with a higher sensor performance of 1.51 rad, a length of 358.95 cm, and maximum initial curvature of 0.49 rad/cm.

Figure 15 is a 3-D view of the initial placement and updated placement after 9000 generations of the GA iteration. We can also see clearly that the initial placement of the fiber-optic sensor is less efficient due to the fact that one part of the sensing fiber is in an unperturbed region. After 9000 generations of the GA iteration, that part of the sensing fiber approaches deeper to the perturbed region.

However, the whole GA process is very slow and does not appear to have reached the global solution because a very low mutation rate is used and the binary representation of the real design variables limits the design space.

Although the previous square panel examples deal with a single dominant *global* deformation mode/case with one and four symmetry lines and therefore, the placement of the optical fiber favors the orientation with the maximum bending curvature, the vital signals such as patient's breathing and heart beat only perturb a small part of the bed mattress. This example shows that the GA-based NURBS curve design procedure has the capability to place the optical sensor to the perturbed location.

IV. Conclusions

In this paper, we present methodology for the placement optimization of both discretely and continuously distributed fiber-optic sensors, in which many point or quasi-point sensors can be multiplexed along a single optical fiber.

A unified SPM is defined for vibration monitoring and fault detection as the integration/summation of a weighted functional of some strain measure over the optical fiber length for both discretely and continuously distributed fiber-optic sensors.

The optical fiber is represented by a NURBS curve. The design variables include the control point coordinates of the NURBS curve and the arclength coordinates of the point sensing element positions along the fiber.

The constraints common to all kinds of optical sensors include the maximum fiber length and maximum allowed initial curvature. The constraints are treated as the exact penalty functions in the fitness function for any GA. We point out that when the total fiber length and the span that the optical fiber covers are much longer than the minimum allowed curvature radius, the constraint on the initial curvature of the fiber curve can be ignored during the optimization. Therefore, the sharp corners are allowed along the fiber curve. This treatment can speed up the convergence. After the optimization, the sharp corners can be treated as a final finish according to the minimum allowed curvature radius.

For discretely distributed fiber-optic sensors, we briefly show by a damage monitoring example how to use a GA-based TSP solver to optimally connect those optimally distributed sensors using one single optical fiber by minimizing the total fiber length. The discrete sensors can be first optimally placed using any proper method though the optimal Latin hypercube sampling is used as the optimality criterion considering the uniformly distributed damage probability density.

For continuously distributed fiber-optic sensors, two sets of examples are given as applications to fluttering or vibrating panels in aerospace engineering using a real-valued GA and a clinical smart bed for patient vital signal monitoring in biomedical engineering using a binary GA. In both cases, the integrating bend-sensing fiber-optic sensors were used.

In all examples, a single deformation mode or case is used to demonstrate the existence of multiple solutions, which justifies using global optimizers such as GAs to optimally place the fiber-optic sensors, and the capability of the GA-based NURBS curve design to directionally and positionally place distributed-sensing optical fibers to improve the sensor performance. However, the binary GA demonstrates a slower convergence than the real-valued GA.

The further work includes 1) combining real-valued multimodal GAs with gradient-based methods to increase the convergence rate, 2) using more control points to enhance the design space, 3) considering multiple vibrating modes or multiple deformation/loading cases using multi-objective GAs, 4) using other sensor performance metrics, including Fisher's information based on various kinds of application fields, and 5) considering the material nonlinearity for the smart bed mattress.

Acknowledgments

The authors gratefully acknowledge the financial support provided for this project by the Carilion Biomedical Institute, and assistance provided by the Carilion Health System Sleep Center and ADMMicro, Inc.

References

[1] Abdullah, M. M., Richardson, A., and Hanif, J., "Online Monitoring of Highway Bridge Construction Using Fiber Bragg Grating Sensors," *Earthquake Engineering and Structural Dynamics*, Vol. 30, No. 8, 2001, pp. 1167–1184. doi:10.1002/eqe.57

[2] Guo, H.-Y., Zhang, L., Zhang, L.-L., and Zhou, J.-X., "Optimal Placement of Sensors for Structural Health Monitoring Using Improved Genetic Algorithms," *Smart Materials and Structures*, Vol. 13, No. 3, 2004, pp. 528–534. doi:10.1088/0964-1726/13/3/011

[3] Prosser, W. H., "Development of Structural Health Management Technology for Aerospace Vehicles," NASA 2003-jannaf-whp, 2003.

[4] Padula, S. L., and Kincaid, R. K., "Optimization Strategies for Sensor and Actuator Placement," NASA TM-1999-209126, 1999.

[5] Yu, T. K., and Seinfeld, J. H., "Observability and Optimal Measurement Location in Linear Distributed Parameter Systems," *International Journal of Control*, Vol. 18, No. 4, 1973, pp. 785–799. doi:10.1080/00207177308932556

[6] Shah, P. C., and Udwadia, F. E., "A Methodology for Optimal Sensor Locations for Identification of Dynamic Systems," *Journal of Applied Mechanics*, Vol. 45, No. 1, 1978, pp. 188–196.

[7] Udwadia, F. E., and Garba, J. A., "Optimal Sensor Locations for Structural Identification," *Proceedings of JPL Workgroup on Identification and Control of Flexible Space Structures*, NASA/JPL, Pasadena, CA, 1985, pp. 247–261.

[8] Kammer, D. C., "Sensor Placements for On-Orbit Modal Identification and Correlation of Large Space Structures," *Journal of Guidance, Control, and Dynamics*, Vol. 14, No. 2, 1991, pp. 251–259.

[9] Kammer, D. C., "Effect of Model Error on Sensor Placement for On-Orbit Modal Identification of Large Space Structures," AIAA Paper 1991-1180, 1991.

[10] Kammer, D. C., and Brillhart, R. D., "Optimal Sensor Placement for Modal Identification Using System-Realization Methods," AIAA Paper 1994-1730, 1994.

[11] Kirkegaard, P. H., and Brincker, R., "On the Optimal Location of Sensors for Parametric Identification of Linear Structural Systems," *Mechanical Systems and Signal Processing*, Vol. 8, No. 6, 1994, pp. 639–647. doi:10.1006/mssp.1994.1045

[12] Meo, M., and Zumpano, G., "On the Optimal Sensor Placement Techniques for a Bridge Structure," *Engineering Structures*, Vol. 27, No. 10, 2005, pp. 1488–1497. doi:10.1016/j.engstruct.2005.03.015

[13] Li, D. S., Li, H. N., and Fritzen, C. P., "The Connection Between Effective Independence and Modal Kinetic Energy Methods for Sensor Placement," *Journal of Sound and Vibration*, Vol. 305, Nos. 4–5, 2007, pp. 945–955. doi:10.1016/j.jsv.2007.05.004

[14] Kammer, D. C., "Sensor Set Expansion for Modal Vibration Testing," *Mechanical Systems and Signal Processing*, Vol. 19, No. 4, 2005, pp. 700–713. doi:10.1016/j.ymssp.2004.06.003

[15] Watanabe, K., Sasaki, M., and Himmelblau, D. M., "Determination of Optimal Measuring Sites for Fault Detection of Non-Linear Systems," *International Journal of Systems Science*, Vol. 16, No. 11, 1985, pp. 1345–1364. doi:10.1080/00207728508926756

[16] Hemez, F. M., and Farhat, C., "An Energy Based Optimum Sensor Placement Criterion and Its Application to Structure Damage Detection," *Proceedings of the 12th International Modal Analysis Conference*, Society for Experimental Mechanics, Honolulu, HI, 1994.

[17] Cobb, R. G., and Liebst, B. S., "Sensor Placement and Structural Damage Identification from Minimal Sensor Information," *AIAA Journal*, Vol. 35, No. 2, 1997, pp. 369–374.

[18] Shi, Z. Y., Law, S. S., and Zhang, L. M., "Optimum Sensor Placement for Structural Damage Detection," *Journal of Engineering Mechanics*, Vol. 126, No. 11, 2000, pp. 1173–1179. doi:10.1061/(ASCE)0733-9399(2000)126:11(1173)

[19] Worden, K., and Burrows, A. P., "Optimal Sensor Placement for Fault Detection," *Engineering Structures*, Vol. 23, No. 8, 2001, pp. 885–901. doi:10.1016/S0141-0296(00)00118-8

[20] Patan, M., and Patan, K., "Optimal Observation Strategies for Model-Based Fault Detection in Distributed Systems," *International Journal of Control*, Vol. 78, No. 18, 2005, pp. 1497–1510. doi:10.1080/00207170500366077

[21] Papadimitriou, C., Beck, J. L., and Au, S.-K., "Entropy-Based Optimal Sensor Location for Structural Model Updating," *Journal of Vibration and Control*, Vol. 6, No. 5, 2000, pp. 781–800. doi:10.1177/107754630000600508

[22] Frecker, M. I., "Recent Advances in Optimization of Smart Structures and Actuators," *Journal of Intelligent Material Systems and Structures*, Vol. 14, Nos. 4–5, 2003, pp. 207–216. doi:10.1177/1045389X03031062

[23] Gawronski, W., and Lim, K. B., "Balanced Actuator and Sensor Placement for Flexible Structures," *International Journal of Control*, Vol. 65, No. 1, 1996, pp. 131–145. doi:10.1080/00207179608921690

[24] Lim, K. B., "Disturbance Rejection Approach to Actuator and Sensor Placement," *Journal of Guidance, Control, and Dynamics*, Vol. 20, No. 1, 1997, pp. 202–204.

[25] Friswell, M. I., "On the Design of Modal Actuators and Sensors," *Journal of Sound and Vibration*, Vol. 241, No. 3, 2001, pp. 361–372. doi:10.1006/jsvi.2000.3300

[26] Mukherjee, A., and Joshi, S., "Piezoelectric Sensor and Actuator Spatial Design for Shape Control of Piezolaminated Plates," *AIAA Journal*, Vol. 40, No. 6, 2002, pp. 1204–1210.

[27] Prosser, W. H., Brown, T. L., Woodard, S. E., Fleming, G. A., and Cooper, E. G., "Sensor Technology for Integrated Vehicle Health

Management of Aerospace Vehicles," *Review of Progress in Quantitative Nondestructive Evaluation: Volume 22*, AIP Conference Proceedings, Vol. 657, AIP, Bellingham, WA, 2003, pp. 1582–1589.

[28] Davis, M. A., Kersey, A. D., Sirkis, J., and Friebele, E. J., "Shape and Vibration Mode Sensing Using a Fiber Optic Bragg Grating Array," *Smart Materials and Structures*, Vol. 5, No. 6, 1996, pp. 759–765. doi:10.1088/0964-1726/5/6/005

[29] Gill, A. S., "Reconstruction of Optical Fiber Bragg Grating Sensor Strain Distributions Using a Genetic Algorithm," M.S. Thesis, North Carolina State University, Raleigh, NC, 2003.

[30] Tsamasphyros, G. J., Furnarakis, N. K., Kanderakis, G. N., and Marioli-Riga, Z. P., "Three-Dimensional Finite Element Analysis of Composite Patches with Embedded Optical Fibres Through Thickness Optimization," *International Conference on Computational & Experimental Engineering and Sciences 01*, ICCES, Puerto Vallarta, Mexico, 2001.

[31] Tsamasphyros, G. J., Kanderakis, G. N., Furnarakis, N. K., Marioli-Riga, Z. P., Chemama, R., and Bartolo, R., "Selection of Optical Fibers Paths and Sensor Locations for Monitoring the Integrity of Composite Patching," *Applied Composite Materials*, Vol. 10, No. 6, 2003, pp. 331–338. doi:10.1023/A:1025791424307

[32] Tsamasphyros, G. J., Kanderakis, G. N., Vrettos, C., and Kalkanis, K., "Numerical Investigation of the Optimum Placement Locations of Optical Fiber Bragg Grating Sensors for the Health Monitoring of Bonded Composite Repairs," *Macromolecular Symposia*, Vol. 247, No. 1, 2007, pp. 221–229. doi:10.1002/masy.200750125

[33] Miller, R. E., "Optimal Sensor Placement via Gaussian Quadrature," *Applied Mathematics and Computation*, Vol. 97, No. 1, 1998, pp. 71–97. doi:10.1016/S0096-3003(97)10120-5

[34] Hiramoto, K., Doki, H., and Obinata, G., "Optimal Sensor/Actuator Placement for Active Vibration Control Using Explicit Solution of Algebraic Riccati Equation," *Journal of Sound and Vibration*, Vol. 229, No. 5, 2000, pp. 1057–1075. doi:10.1006/jsvi.1999.2530

[35] Wouwer, A. V., Point, N., Porteman, S., and Remy, M., "An Approach to the Selection of Optimal Sensor Locations in Distributed Parameter Systems," *Journal of Process Control*, Vol. 10, No. 4, 2000, pp. 291–300. doi:10.1016/S0959-1524(99)00048-7

[36] Thite, A. N., and Thompson, D. J., "Selection of Response Measurement Locations to Improve Inverse Force Determination," *Applied Acoustics*, Vol. 67, No. 8, 2006, pp. 797–818. doi:10.1016/j.apacoust.2006.01.001

[37] Yao, L., Sethares, W. A., and Kammer, D. C., "Sensor Placement for On-Orbit Modal Identification via a Genetic Algorithm," *AIAA Journal*, Vol. 31, No. 10, 1993, pp. 1922–1928.

[38] Holland, J., *Adaptation in Natural and Artificial Systems*, The University of Michigan Press, Ann Arbor, MI, 1975.

[39] Michalewicz, Z., *Genetic Algorithms + Data Structures = Evolution Programs*, AI Series, Springer–Verlag, New York, 1994.

[40] Zhang, H., Lennox, B., Goulding, P. R., and Leung, A. Y.-T., "A Float-Encoded Genetic Algorithm Technique for Integrated Optimization of Piezoelectric Actuator and Sensor Placement and Feedback Gains," *Smart Materials and Structures*, Vol. 9, No. 4, 2000, pp. 552–557. doi:10.1088/0964-1726/9/4/319

[41] Spillman, W. B., Jr., Kline, B. R., Maurice, L. B., and Fuhr, P. L., "Statistical-Mode Sensor for Fiber-Optic Vibration Sensing Uses," *Applied Optics*, Vol. 28, No. 15, 1989, pp. 3166–3176.

[42] Huston, D. R., Fuhr, P. L., Beliveau, J. G., and Spillman, W. B., Jr., "Structural Member Vibration Measurements Using a Fiber Optic Sensor," *Journal of Sound and Vibration*, Vol. 149, No. 2, 1991, pp. 348–353. doi:10.1016/0022-460X(91)90645-Z

[43] Cox, D. E., and Lindner, D. K., "Active Control for Vibration Suppression in a Flexible Beam Using a Modal Domain Optical Fiber Sensor," *Journal of Vibration and Acoustics*, Vol. 113, No. 3, 1991, pp. 369–382.

[44] Vengsarkar, A. M., Fogg, B. R., Miller, W. V., Murphy, K. A., and Claus, R. O., "Elliptical-Core, Two-Mode Optical Fibre Sensors as Vibration-Mode Filters," *Electronics Letters*, Vol. 27, No. 11, 1991, pp. 931–932. doi:10.1049/el:19910582

[45] Bock, W. J., Porada, E., and Zaremba, M. B., "Neural Processing-Type Fiber-Optic Strain Sensor," *IEEE Transactions on Instrumentation and Measurement*, Vol. 41, No. 6, 1992, pp. 1062–1066. doi:10.1109/19.199397

[46] Murphy, K. A., Fogg, B. R., and Vengsarkar, A. M., "Spatially Weighted Vibration Sensors Using Tapered Two-Mode Optical Fibers," *Journal of Lightwave Technology*, Vol. 10, No. 11, 1992, pp. 1680–1687. doi:10.1109/50.184908

[47] Lindner, D. K., Zvonar, G. A., Baumann, W. T., and Delos, P. L., "Nonlinear Effects of a Modal Domain Optical Fiber Sensor in a Vibration Suppression Control Loop for a Flexible Structure," *Journal of Vibration and Acoustics*, Vol. 115, No. 1, 1992, pp. 120–128.

[48] Han, L., Voloshin, A., and Coulter, J., "Application of the Integrating Fiber Optic Sensor for Vibration Monitoring," *Smart Materials and Structures*, Vol. 4, No. 2, 1995, pp. 100–105. doi:10.1088/0964-1726/4/2/005

[49] Spillman, W. B., Jr., and Huston, D. R., "Scaling and Antenna Gain in Integrating Fiber-Optic Sensors," *Journal of Lightwave Technology*, Vol. 13, No. 7, 1995, pp. 1222–1230. doi:10.1109/50.400695

[50] Yu, F. T., Pan, K., Zhao, D., and Ruffin, P. B., "Fiber Vibration Sensor That Uses the Speckle Contrast Ratio," *Optical Engineering*, Vol. 34, No. 1, 1995, pp. 236–239. doi:10.1117/12.188329

[51] Spillman, W. B., Jr., Mayer, M., Bennett, J., Gong, J., Meissner, K. E., Davis, B., Claus, R. O., Muelenaer, A. A., Jr., and Xu, X., "A 'Smart' Bed for Non-Intrusive Monitoring of Patient Physiological Factors," *Measurement Science and Technology*, Vol. 15, July 2004, pp. 1614–1620. doi:10.1088/0957-0233/15/8/032

[52] Xu, J., "Dual Processing Spatially Distributed Integrating Fiber Optic Sensors for Non-intrusive Patient Monitoring," M.S. Thesis, Physics Department, Virginia Polytechnic Institute and State University, Blacksburg, VA, 2005.

[53] Gauthier, R. C., and Ross, C., "Theoretical and Experimental Considerations for a Single-Mode Fiber-Optic Bend-Type Sensor," *Applied Optics*, Vol. 36, No. 25, 1997, pp. 6264–6273.

[54] Wan, K. T., and Leung, C. K. Y., "Fiber Optic Sensor for the Monitoring of Mixed Mode Cracks in Structures," *Sensors and Actuators A, Physical*, Vol. 135, No. 2, 2007, pp. 370–380. doi:10.1016/j.sna.2006.08.002

[55] Xu, Y., Jones, N., Fothergill, J., and Hanning, C., "Error Analysis of Two-Wavelength Absorption-Based Fibre-Optic Sensors," *Optics and Lasers in Engineering*, Vol. 36, No. 6, 2001, pp. 607–615. doi:10.1016/S0143-8166(01)00062-8

[56] Leung, C. K. Y., Olson, N., Wan, K. T., and Meng, A., "Theoretical and Experimental Investigations of Macro-Bend Losses for Standard Single Mode Fibers," *Journal of Engineering Mechanics*, Vol. 131, No. 8, 2005, pp. 777–790. doi:10.1061/(ASCE)0733-9399(2005)131:8(777)

[57] Wang, Q., Farrell, G., and Freir, T., "Theoretical and Experimental Investigations of Macro-Bend Losses for Standard Single Mode Fibers," *Optics Express*, Vol. 13, No. 12, 2005, pp. 4476–4484. doi:10.1364/OPEX.13.004476

[58] Wang, Q., Rajan, G., Wang, P., and Farrell, G., "Polarization Dependence of Bend Loss for a Standard Singlemode Fiber," *Optics Express*, Vol. 15, No. 8, 2007, pp. 4909–4920. doi:10.1364/OE.15.004909

[59] Carrara, S. L. A., Almeida, S. F. M., Covington, C. E., and Blake, J. N., "Modeling of the Bend Sensitivity of Asymmetrical-Core Two-Mode Fiber Interferometers," *Journal of the Optical Society of America A*, Vol. 12, No. 5, 1995, pp. 869–880.

[60] Kulchin, Y. N., Vitrik, O. B., and Perfilyev, V. G., "Sensitive Element and Quasi-Distributed Fiber Optic Sensor for Bending Deformations," *Fiber Optic Sensor Technology and Applications*, Proc. SPIE Vol. 3860, edited by M. A. Marcus, and Brian Culshaw, SPIE–International Society for Optical Engineering, Bellingham, WA, 1999, pp. 362–365.

[61] Blanchard, P. M., Burnett, J. G., Erry G., R. G., Greenaway, A. H., Harrison, P., Mangan, B., Knight, J. C., Russell, P. S. J., Gander, M. J., McBride, R., and Jones, J. D. C., "Two-Dimensional Bend Sensing with a Single, Multi-Core Optical Fibre," *Smart Materials and Structures*, Vol. 9, No. 2, 2000, pp. 132–140. doi:10.1088/0964-1726/9/2/302

[62] Klute, S. M., Duncan, R. G., Fielder, R. S., Butler, G. W., Mabe, J. H., Sang, A. K., Seeley, R. J., and Raum, M. T., "Fiber-Optic Shape Sensing and Distributed Strain Measurements on a Morphing Chevron," AIAA Paper 2006-624, 2006.

[63] Farin, G., *Curves and Surfaces for Computer Aided Geometric Design: A Practical Guide*, 2nd ed., Academic Press, New York, 1990.

[64] Kapania, R. K., and Li, J., "On a Geometrically Exact Curved/Twisted Beam Theory Under Rigid Cross-Section Assumption," *Computa-*

tional Mechanics, Vol. 30, Nos. 5–6, 2003, pp. 428–443. doi:10.1007/s00466-003-0421-8

[65] Kapania, R. K., and Li, J., "A Formulation and Implementation of Geometrically Exact Curved Beam Elements Incorporating Finite Strains and Finite Rotations," *Computational Mechanics*, Vol. 30, Nos. 5–6, 2003, pp. 444–459. doi:10.1007/s00466-003-0422-7

[66] Udd, E., Schulz, W., Seim, J., Corones, J., and Laylor, H. M., "Fiber Optic Sensors for Infrastructure Applications," Oregon Department of Transportation, TR SPR 374 (Final), Feb. 1998.

[67] Pietrzykowski, T., "An Exact Potential Method for Constrained Maxima," *SIAM Journal of Numerical Analysis*, Vol. 6, No. 2, 1969, pp. 299–304.

[68] Houck, C. R., Joines, J. A., and Kay, G. M., "A Genetic Algorithm for Function Optimization: A Matlab Implementation," http://www.ie.ncsu.edu/mirage/GAToolBox/gaot/papers/gaotv5.ps, 1995.

[69] Spink, M., "NURBS Toolbox for SCILAB and MATLAB," http://www.aria.uklinux.net/nurbs.php3 [retrieved 20 April 2005].

[70] Roberts, A. P., and Garboczi, E. J., "Elastic Properties of Model Random Three-Dimensional Open-Cell Solids," *Journal of the Mechanics and Physics of Solids*, Vol. 50, No. 1, 2002, pp. 33–55. doi:10.1016/S0022-5096(01)00056-4

B. Balachandran
Associate Editor